ISSN 1070-3284, Russian Journal of Coordination Chemistry, 2018, Vol. 44, No. 1, pp. 15–20. © Pleiades Publishing, Ltd., 2018.

Synthesis and Optoelectronic Properties of a Pt(II) Complex with 2-Pyridin-2-Yl-1,3-Thiazole-4-Carboxylic Acid[1]

X. P. Zhang[a, b], D. S. Zhang[a, b], W. Sun[a, b], and Z. F. Shi[a, b, *]

[a] *College of Chemistry and Chemical Engineering, Hainan Normal University, Haikou, 571158 P.R. China*

[b] *Key Laboratory of Water Pollution Treatment & Resource Reuse of Hainan Province, Haikou, 571158 P.R. China*

**e-mail: zaifengshi_hnnu@sina.com*

Received March 20, 2017

Abstract—A carboxyl functionalized Pt(II) complex $PtC_9H_6N_2O_2SCl_2$ (**I**) has been synthesized by the coordination reaction of K_2PtCl_4 with 2-pyridin-2-yl-1,3-thiazole-4-carboxylic acid. The absorption property and photosensitizing performance of **I** has been studied. Through assembling the dye-sensitized solar cells (DSSCs) based on complex **I**, a weak solar-energy-to-electricity conversion is presented. Additionally, when complex **I** was solved in DMF solution, a novel complex $PtC_9H_7N_2O_3SCl$ (**II**) could be obtained. The structure of **II** has been confirmed by the single-crystal X-ray diffraction (CIF file CCDC no. 1538911).

Keywords: Pt(II) complex, crystal structure, optoelectronic properties, density functional theory (DFT)

DOI: 10.1134/S1070328418010098

INTRODUCTION

Platinum(II) complexes have received considerable interest due to their intriguing chemical and physical properties. In the past decades, great work has been devoted to emitting devices and environment-responsive smart materials based on Pt(II) complexes [1, 2]. Square-planar configurations have been always exhibited for Pt(II) complexes, and these planar molecules are susceptible to aggregation in oligomers through intermolecular Pt···Pt and/or π–π interactions, leading to interesting changes in color, luminescence and so on [3]. Besides, due to planar structures, Pt(II) complexes are endowed with good charge-transfer properties that can be feasibly tuned by variation of electron-withdrawing or electron-donating groups of ligands, usually showing an intense metal-to-ligand-charge-transfer (MLCT) absorptions in the visible region [4]. Consequently, planar Pt(II) complexes can be served as an efficient photosensitizer to promote charge separation [5].

Dye-sensitized solar cell (DSSC) is one of the hot research fields. Photosensitizer is an important and indispensable component of DSSCs, and much attention has been paid to the designing and synthesizing of sensitizers. Transition-metal complexes with polypyridine ligands always present intense charge-transfer (CT) absorptions with large extinction coefficients, which is conducive to light absorption and charge separation/transport. Utilizing transition-metal complexes as photosensitizers, a great deal of DSSCs have been extensively reported, especially for ruthenium(II) polypyridine and zinc porphyrin complexes. The DSSCs fabricated by the famous black dye $[RuL(NCS)_3]^-$ and YD2-*o*-C8, showed efficiencies of as high as 10.4 and 12.3%, respectively [6, 7]. Sensitizing behaviors of donor–acceptor platinum(II) polypyridylalkynyl complexes also have been studied, and a power-conversion efficiency of 3.6% has been obtained [8].

In previous studies, we have investigated environment-responsive behaviors of chiral Pt(II) complexes. Different color, luminescent and chiroptical properties were exhibited in the vapor-, mechano-, solvent-, and temperature-induced structural transformation processes [9–12]. In this work, a Pt(II) complex $PtC_9H_6N_2O_2SCl_2$ (**I**) with 2-pyridin-2-yl-1,3-thiazole-4-carboxylic acid has been prepared and the photosensitizing behavior have been explored. Interestingly, when **I** was solved in DMF solution, a novel complex $PtC_9H_7N_2O_3SCl$ (**II**) could be obtained, which was confirmed by the single-crystal X-ray diffraction.

EXPERIMENTAL

General methods. All reagents were purchased from commercial suppliers and used as received. Mass spectra were acquired on an LCQ Fleet ESI mass spectrometer. The NMR spectra were obtained on Bruker DRX-400 spectrometer. Chemical shifts are referenced to TMS. Coupling constants are given in hertz.

[1] The article is published in the original.

UV-Vis spectra were measured on a UV-3600 spectrophotometer.

Synthesis. Based on a previous study [13], complex **I** was easily prepared by the coordination reaction of K_2PtCl_4 with 2-pyridin-2-yl-1,3-thiazole-4-carboxylic acid in refluxed HCl (0.2 M) solution for 5 h under argon atmosphere (Scheme 1).Yellow precipitates were filtrated and washed with water and methanol. The yield was 81%.

^{1}H NMR (400 MHz; DMSO; δ, ppm): 8.68 (m., 1H), 8.60 (s., 1H), 8.16 (dt., J_1 = 8.0 Hz, J_2 = 1.0 Hz, 1H), 8.02 (td., J_1 = 8.0 Hz, J_2 = 1.0 Hz, 1H), 7.56 (m, 1H). ^{13}C NMR (100 MHz; DMSO; δ, ppm): 168.8, 162.0, 149.8, 149.7, 148.4, 138.0, 130.8, 125.7, 119.4. MS (ESI) (*m/z*): 471 [M^- – 1].

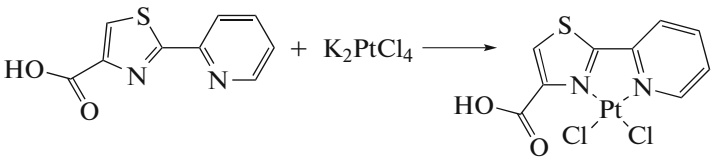

Scheme 1.

X-ray structure determination. Single-crystal X-ray diffraction measurements were carried out on a Bruker SMART APEX CCD based on diffractometer operating at room temperature. Intensities were collected with graphite monochromatized MoK_α radiation (λ = 0.71073 Å) operating at 50 kV and 30 mA, using ω/2θ scan mode. The data reduction was made with the Bruker SAINT package [14]. Absorption corrections were performed using the SADABS program [15]. The structures were solved by direct methods and refined on F^2 by full-matrix least-squares using SHELXL-97 with anisotropic displacement parameters for all non-hydrogen atoms in all two structures. Hydrogen atoms bonded to the carbon atoms were placed in calculated positions and refined as riding mode with C–H = 0.93 Å (methane) or 0.96 Å (methyl) and U_{iso}(H) = 1.2U_{eq} ($C_{methane}$) or U_{iso}(H) = 1.5U_{eq}(C_{methyl}). The water hydrogen atoms were located in the difference Fourier maps and refined with an O–H distance restraint (0.85(1) Å) and U_{iso}(H) = 1.5 U_{eq}(O). All computations were carried out using the SHELXTL-97 program package [16]. Crystallographic data for complex **II** are summarized in Table 1. The coordinate bond lengths and angles are summarized in Table 2.

Supplementary material for structure **II** has been deposited with the Cambridge Crystallographic Data Centre (CCDC no. 1538911; deposit@ccdc.cam.ac.uk or http://www.ccdc.cam.ac.uk).

Computational details. For the calculation, the geometry of **I** was fully optimized without any symmetry constraints. The effect of the solvent was modeled by the CPCM dielectric model with dichloromethane solution. The B3LYP functional was adopted, and the 18-valence electron Stuttgart small core relativistic pseudo-potentials with their corresponding optimized set of basic functions were employed for the Pt atom [17], while the standard split-valence 6-31G* basis set was used for all other atoms. All the calculations were carried out using the Gaussian03 program [18].

RESULTS AND DISCUSSION

As shown in Fig. 1, the UV-Vis absorption of complex **I** has been measured. A series of intense absorption bands in the region of 220–320 nm can be attributed to characteristic intraligand (IL) transitions (n–π* and π–π*) of 2-pyridin-2-yl-1,3-thiazole-4-carboxylic acid. The low-energy absorptions locating at 320–450 nm are stemmed from MLCT transitions and ligand-to-ligand charge transfer transitions (LLCT) [19]. The calculations of frontier molecular orbitals and UV-Vis spectrum also have been performed. The highest occupied molecular orbital (HOMO) and the lowest unoccupied molecular orbital (LUMO) energies of **I** are calculated to be –5.997 and –3.308 eV, respectively (Fig. 2). The LUMO is mainly located on 2-pyridin-2-yl-1,3-thiazole-4-carboxylic acid ligand, while the HOMO is mainly located on Pt(II) nucleus two Cl^- anions. As a consequence, MLCT and LLCT transitions contribute to the low-energy absorptions of **I** to a large extent. The simulated UV-Vis spectrum from TD-DFT calculations of **I** is in good agreement with the experimental result with regard to the shape, and low-energy absorptions of both calculation and experiment tail down to ~450 nm.

DSSCs based on complex **I** were fabricated according to the literature [20, 21], and photosensitizing behavior of complex **I** has been explored (Fig. 3). The short-circuit photocurrent density (J_{sc}) is 0.66 mA/cm^2, and the open-circuit potential (V_{oc}) is 0.338 V. While a weak solar-energy-to-electricity conversion yield value (η = 0.12) is presented, which is in accordance with the weak absorption of low-energy band (300–500 nm) of complex **I**.

Table 1. Crystallographic data and structure refinements for complex **II**

Parameter	Value
Formula	$C_9H_7N_2O_3SClPt \cdot H_2O$
Mr	471.78
Crystal system	Triclinic
Space group	$P\bar{1}$
a, Å	7.476(2)
b, Å	8.987(3)
c, Å	9.627(3)
α, deg	84.006(4)
β, deg	72.601(4)
γ, deg	79.161(3)
V, Å^3	605.4(3)
Z	2
T, K	273(2)
Radiation, λ, Å	0.71073
ρ_{calcd}, g/cm^{-3}	2.588
μ, mm^{-1}	11.988
F(000)	440
Reflections collected	3319
Unique reflections (R_{int})	2388 (0.0219)
GOOF (F^2)	1.017
R_1, wR_2 ($I > 2\sigma(I)$)	0.0270, 0.0712
R_1, wR_2 (all data)	0.0277, 0.0717

Table 2. Structural parameters determined by X-ray single crystal diffraction

Bond	*d*, Å	Angles	ω, deg
Pt(1)–N(1)	2.002(5)	N(1)Pt(1)N(2)	81.67(19)
Pt(1)–N(2)	2.055(5)	N(1)Pt(1)O(1)	179.32(15)
Pt(1)–O(1)	2.029(4)	N(1)Pt(1)Cl(1)	93.79(15)
Pt(1)–Cl(2)	2.2802(15)	N(2)Pt(1)O(1)	98.72(18)
		N(2)Pt(1)Cl(1)	175.44(12)
		O(1)Pt(1)Cl(1)	85.81(14)

When complex **I** was solved in DMF solution, a substitution reaction would occur slowly. Due to the weak basicity of DMF solution [22], the hydrogen atom of 2-pyridin-2-yl-1,3-thiazole-4-carboxylic acid could be neutralized. In this case, to maintain electrical neutrality, one chloride anion was replaced with a water molecule. The proposed reaction process is shown in Scheme 2.

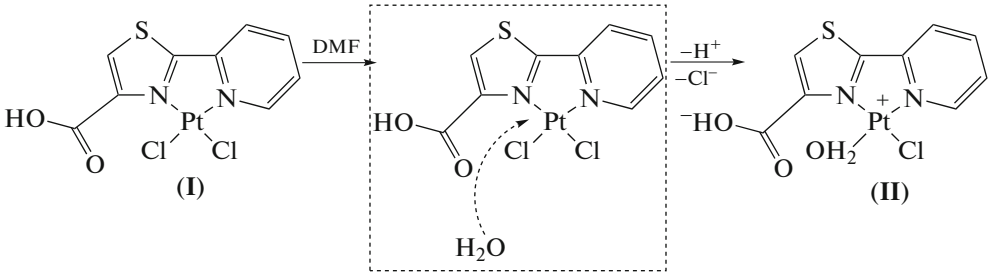

Scheme 2.

A few single crystals have been obtained by slow evaporation of DMF solution of complex **I** at 273K, and the structure of complex **II** is confirmed by the single-crystal X-ray diffraction. The crystal structure of **II** crystallizes in $P\bar{1}$ space group of triclinic system (Table 1) with one complex molecule and a co-crystallized water molecule per asymmetrical unit (Fig. 4). The Pt(II) nucleus is coordinated by two nitrogen atoms of 2-pyridin-2-yl-1,3-thiazole-4-carboxylic acid, one chloride anion and one oxygen atom of coordinated water molecule, showing a square-planar configuration. Selected bond lengths and chelating bite angles around central Pt^{2+} ion of complex **II** are in accordance with the corresponding structural parameters of Pt(II) complexes reported before [23, 24]. The Pt–N bond lengths vary from 2.002(5) to 2.055(5) Å. Pt–Cl bond is 2.2802(15) Å and Pt–O bond is 2.029(4)Å. The bite angles of N(1)Pt(1)N(2) and Cl(1)Pt(1)O(1) are 81.67(19)° and 85.81(14)°, respectively.

As shown in Fig. 5, the molecules of **II** are arranged into one-dimensional chain in a head-to-tail pattern along *z* axis, and dimers are formed through weak π–π

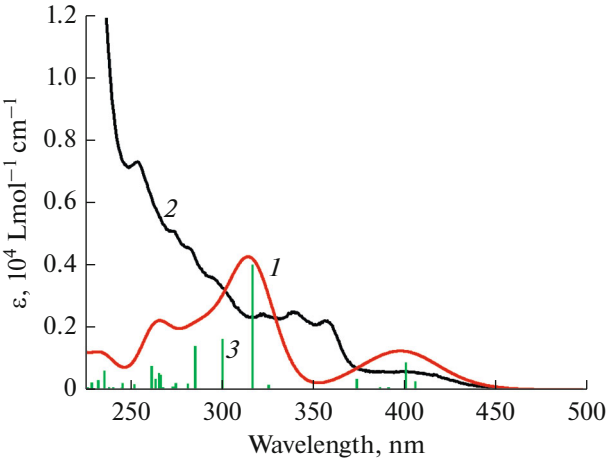

Fig. 1. Computed UV-Vis spectrum of complexes **I** in dichloromethane solution (*1*) compared to experiment (5×10^{-5}mol L^{-1}) (*2*). The column (*3*) is the computed rotatory strength.

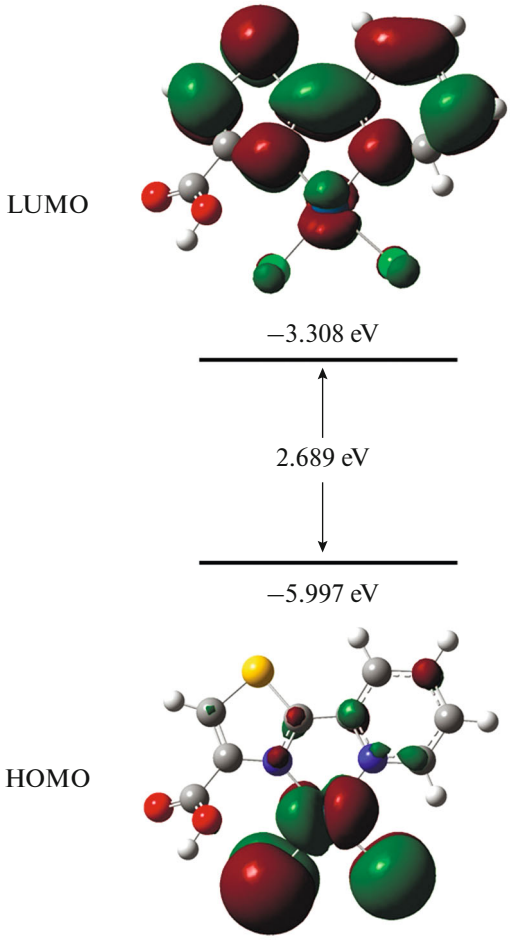

Fig. 2. Contour plots of the HOMO and LUMO of **I**.

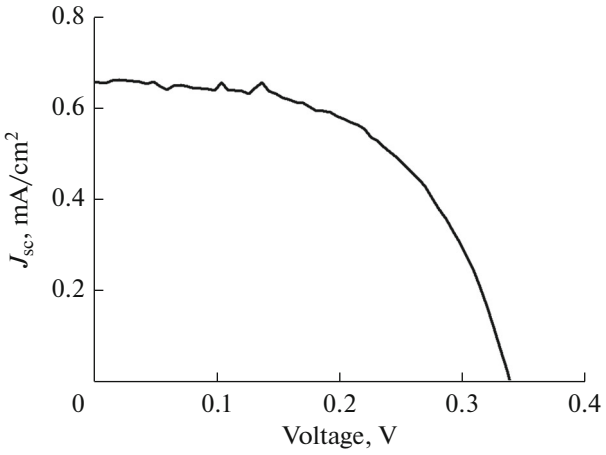

Fig. 3. Photocurrent density-voltage curves of DSSCs based on complex **I**.

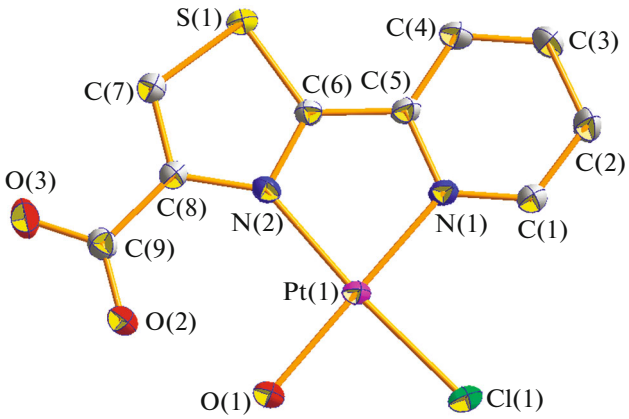

Fig. 4. X-ray crystal structure of **II**. H atoms and solvent molecule are omitted for clarity.

interaction (3.889(1) Å) between adjacent thiazole rings. Distinct hydrogen bonding interactions are exhibited in the crystal structure (Fig. 6). For single complex molecule, intramolecular hydrogen bond

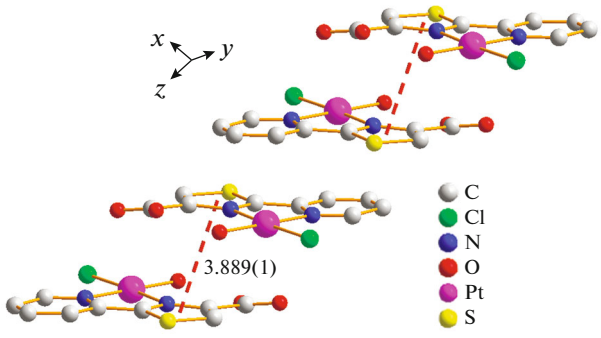

Fig. 5. The packing structure of complex **II** along *z* axis. H atoms and solvent molecules are omitted for clarity.

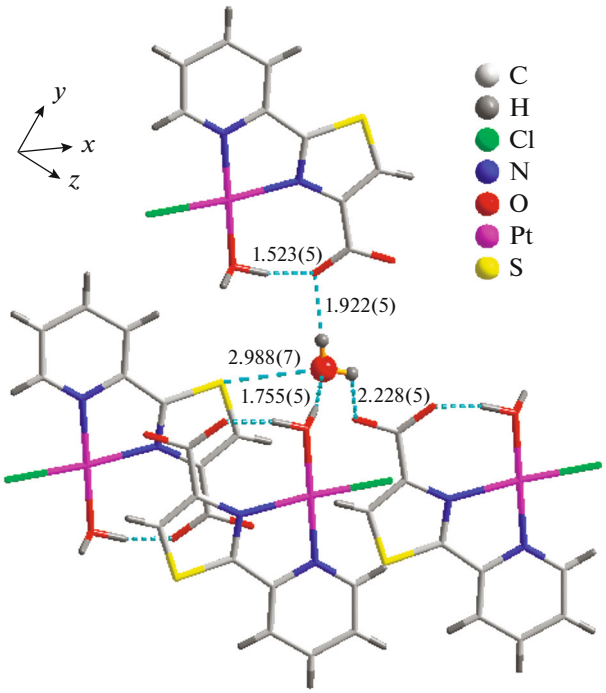

Fig. 6. Hydrogen bonding interactions in crystal structure of complex **II**.

(1.523(5) Å) is formed between the hydrogen atom of coordinated water molecule and the oxygen atom of carboxyl group. In addition, the co-crystallized water molecule serves as a nucleus, and diverse intermolecular hydrogen bonding interactions are formed through it. It can be inferred that both π–π stacking and hydrogen bonding contacts are favorable to the stabilization of the crystal structure of complex **II**.

Thus, the preparation and optoelectronic properties of a Pt(II) complex (**I**) with 2-pyridin-2-yl-1,3-thiazole-4-carboxylic acid have been investigated. A weak solar-energy-to-electricity conversion can be observed, which is consistent with the weak absorption of low-energy band (300–500 nm) of complex **I**. The UV-Vis spectrum also has been simulated, and the low-energy absorptions of **I** mainly come from MLCT and LLCT transitions. In addition, a new complex **II** can be separated by evaporation of DMF solution containing complex **I**. The structure of **II** is affirmed by the single-crystal X-ray diffraction, and one-dimensional chain is formed through distinct π–π interactions.

ACKNOWLEDGMENTS

This work is supported by the National Natural Science Foundation of China (grant no. 21601043), Natural Science Foundation of Hainan Province (nos. 217100, 217101, ZDYF2017011, and 2017CXTD007), the program fund of Department of Science and Tech-

nology of Hainan Province, P.R. China (no. XH201421).

REFERENCES

1. Chan, S.-C., Chan, M.C.W., Wang, Y., et al., *Chem. Eur. J.*, 2001, vol. 7, p. 4180.
2. Genovese, D., Aliprandi, A., and Prasetyanto, E.A., *Adv. Funct. Mater.*, 2016, vol. 26, p. 5271.
3. Gong, Z.-L. and Zhong, Y.-W., *Inorg. Chem.*, 2016, vol. 55, p. 10143.
4. Rodrigue-Witchel, A., Rochester, D.L., and Zhao, S.-B., *Polyhedron*, 2016, vol. 108, p. 151.
5. Dai, F.-R., Chen, Y.-C., Lai, L.-F., et al., *Chem. Asian J.*, 2012, vol. 7, p. 1426.
6. Nazeeruddin, M.K., Pechy, P., Renouard, T., et al., *J. Am. Chem. Soc.*, 2001, vol. 123, p. 1613.
7. Yella, A., Lee, H.-W., Tsao, H.N., et al., *Science*, 2011, vol. 334, p. 629.
8. Kwok, E.C.-H., Chan, M.-Y., Wong, K.M.-C., et al., *Chem. Eur. J.*, 2010, vol. 16, p. 12244.
9. Zhang, X.-P., Wu, T., Liu, J., et al., *J. Mater. Chem., C*, 2014, vol. 2, p. 184.
10. Zhang, X.-P., Mei, J.-F., Lai, J.-C., et al., *J. Mater. Chem., C*, 2015, vol. 3, p. 2350.
11. Zhang, X.-P., Chang, V.Y., Liu, J., et al., *Inorg. Chem.*, 2015, vol. 54, p. 143.
12. Zhang, X.-P., Zhu, L., Wang, X., et al., *Inorg. Chim. Acta*, 2016, vol. 442, p. 56.
13. Kolp, B., Abeln, D., Stoeckli-Evans, H., et al., *Eur. J. Inorg. Chem.*, 2001, p. 1207.
14. *SAINT, Area Detector Control and Integration Software*, Madison: Siemens Analytical X-ray Instruments Inc., 1996.
15. Sheldrick, G.M., *SADABS, Program for Empirical Absorption Correction of Area Detector Data*, Göttingen: Univ. of Göttingen, 1996.
16. Sheldrick, G.M., *SHELXL-97 and SHELXTL, Software Reference Manual, Version 5.1*, Madison: Bruker AXS Inc., 1997.
17. Andrae, D., Haeussermann, U., Dolg, M., et al., *Theor. Chim. Acta*, 1990, vol. 77, p. 123.
18. Frisch, M.J., Trucks, G.W., Schlegel, H.B., et al., *Gaussian 03, Revision E.01*, Wallingford CT, Gaussian, Inc., 2004.
19. Hissler, M., Connick, W.B., Geiger, D.K., et al., *Inorg. Chem.*, 2000, vol. 39, p. 447.
20. Liu, J., Wang, K., Zhang, X., et al., *Tetrahedron*, 2013, vol. 69, p. 190.
21. Ma, B.-B., Peng, Y.-X., Tao, T., et al., *Dyes Pigm.*, 2015, vol. 117, p. 100.
22. Liu, J.-J., Shan, Y.-B., Fan, C.-R., et al., *Inorg. Chem.*, 2016, vol. 55, p. 3680.
23. He, X.-F., Vogels, C.M., Decken, A., et al., *Polyhedron*, 2004, vol. 23, p. 155.
24. Brooks, J., Babayan, Y., Lamansky, S., et al., *Inorg. Chem.*, 2002, vol. 41, p. 3055.